Chapter 6

Pyrolysis of Sugarcane Leaves (*Saccharum officinarum L*): Kinetics of Thermal Degradation Process and Product Characterization

Abstract

Pyrolysis of sugarcane (*Saccharum officinarum* L) leaves (SCL) has been investigated using DTA/TGA unit and a fixed bed batch pyrolyser. Proximate and ultimate analyses and calorific value measurement have been carried out using standard protocols. The kinetic analysis of pyrolysis has been carried using iso-conversional model free methods as well as multiple linear regression method. Apparent activation energy values evaluated from iso-conversional methods have ranged from 214.9 to 239.6kJ/mol where as in the case of multiple linear regression analysis it has ranged from 25.06 to 57.23kJ/mol. The multi-step reaction mechanism has been investigated using the Criado method. Slow pyrolysis has been used to collect the pyrolytic product. Effects of pyrolysis process parameter such as temperature, heating rate (15-30^{o}C/min), bed height (4-16cm) and particle size (0.710-0.180mm) have been studied. The maximum bio-oil and bio-char yields are found to be 44.78% (550^{o}C) and 36.82% (350^{o}C), respectively. Physicochemical properties of bio-oil are compared with the diesel oil. Chemical constituents are identified using FTIR, ^{1}HNMR and GC–MS techniques. The bio-char has been characterized using proximate, ultimate, HHV, FTIR, SEM-EDX, ICP-AES, BET surface area and XRD analyses. The GC-MS analysis of bio-oil has confirmed the presence of aromatic derivatives, phenols, ketones, and oxygenated compounds of high molecular weight that may be separated as useful chemical products. The pyrolytic gases are analysed using gas chromatography. With increase in pyrolysis temperature, the composition of hydrogen and hydrocarbons has increased significantly while the formation of carbon dioxide has reduced. High percentage of hydrogen and methane in the product gas and its high HHV (MJ/kg) value has indicated its good fuel value.

6.1 Introduction

Sugar cane (*Saccharum officinarum L*) leaves are a waste biomass left in the cane fields after the harvesting of sugar cane. India is the second largest producer of sugar cane after the Brazil which contributes 25% of the global production (Sindhu et al., 2016). In India, the sugar cane cultivated area is 4.95 million ha and the crop yield is 70.39 tons/ha. Sugarcane crop consists of about 25% leaves and tops and the residue ratio is about 0.33, customarily 1 MT of sugar cane generates 0.2–0.3 MT of sugarcane leaves and tops as waste and is the most surplus available crop residue in India (Charusiri and Vitidsant, 2017; Sindhu et al., 2016). Normally most of it is burnt in the field, and there is no proper and scientific use of this large residue. Further, burning of this waste in the field, releases carbon monoxide, carbon dioxide, sulphur oxides, nitrogen oxides, particulate matter as fly ash and degrades soil microbial diversity (Pasakorn, 2018; Sindhu et al., 2016). Conversion of sugar cane leaves to value added products can be done by using thermo-chemical or biochemical routes. The thermo-chemical process is more appropriate than biochemical process because later process needs long time for conversion into valuable products and is less efficient (Ahmad et al., 2017b; Mishra and Mohanty, 2018). Pyrolysis is the most potential process to convert biomass into solid, liquid and gaseous form among other thermochemical processes. It is highly dependent upon various parameters such as biomass composition and nature, heating rate, temperature, residence time, moisture content and particle size (Müsellim et al., 2018). To convert the abundant availability of biomass like sugar cane leaves through pyrolysis to condensable products (bio-oil), syngas and solid (char) efficiently, it is essential to know the kinetics of thermal decomposition process and

the nature of degradation products. In view of this the thermal degradation behaviour of sugar cane leaves has been investigated in detail in this work.

6.2 Sample collection and preparation

Sample of sugarcane leaves (SCL) were collected from the fields of sugarcane, located in Lakhimpur Kheri district (26.90°N 81.30°E) of Uttar Pradesh, India. Raw SCL samples were cleaned manually then washed with tap water and sun dried for two days. The sun dried samples were cut into small pieces and further dried in a hot air oven (Universal Oven Model NSW-143(OUA-2)) at 60°C for 24 h. The oven dried samples were pulverized into powdered form in a Wiley Mill (Model 2, Arthur H. Thomas. Co Philadelphia, USA) and was sieved through a mesh screen (size range, 0.300–0.180 mm) in order to obtain a uniform particle size. Powdered biomass sample was stored in an air tight Ziploc poly bag at room temperature to prevent the moisture absorption and use for further characterization and experiments. The raw powdered sample was sieved by employing gyratory sieve shaker (model: KI-133(a)) using different sieve sizes in sequence:> 0.71mm, 0.710-0.425mm, 0.425-0.300mm, 0.300-0.180mm for 15 min to separate as per to their size. These different particle sizes were used further for study of variation of particle size of biomass on bio-oil yield. Bulk densities (kg/m^3) of SCL sample of different sizes were measured in accordance with ASTM Standard Method-873.

6.3 TG and DTG analysis

Pyrolysis of SCL was carried out using a simultaneous thermal analyzer which combines a heat flux type DSC with a TGA (STA 8000 &8500 Perkin Elmer Ltd; having a precision of – temperature: ±0.1K, DSC sensitivity: ±0.1mW and microbalance sensitivity: ±0.1µg), to

obtaining the data of weight loss with time or temperature throughout the pyrolysis reaction. About 10 ± 0.01 mg of powdered SCL sample was placed into alumina crucible and kept to equilibrate at 30°C. The thermal analysis was carried out from 30 to 1000°C using six different non-isothermal heating rates of 5, 10, 15, 20, 30 and 40°C/min to evaluate the kinetic triplets. To avoid unwanted secondary reaction and oxidation of sample, nitrogen gas at a flow rate of 20mL/min was used to create an inert environment into the pyrolysis reaction chamber. To ensure the reproducibility, each experiment was repeated at least twice. The DTG data for samples were obtained from the TGA data using origin pro-software. The differential scanning calorimetry (DSC) experiments were carried out using (STA8000&8500 Perkin Elmer Ltd.) at all the six different hating rates used during TGA study. The heat flow (mW) was recorded with time or temperature during DSC analysis.

6.4 Physical and thermo-chemical characteristics of SCL biomass

Thermochemical characterization of SCL sample were carried out by investigating the parameters such as proximate, ultimate, and biochemical analyses and higher heating value (MJ/kg). These are the vital characterization methods of any raw biomass sample to be used for thermal conversion in to useful end product. Under the proximate analysis, moisture content (MC), volatile matter (VM) and ash content was carried out by using ASTM standard methods. All the experiments were carried out in triplicate and average value are reported as percentage. The fixed carbon (FC) was estimated by the difference using equation:

$$Fixed\ carbon\ (\%) = 100 - \{MC(\%) + VM(\%) + Ash\ content(\%)\} \qquad (6.1)$$

Ultimate analysis (C, H, N and S) was carried out using CHNS analyzer (Euro EA 3000, Elemental Analyzer Riva Del Garda Italy). The percentage of oxygen was obtained by the difference using equation:

$$\%O = 100 - (\%C + \%H + \%N + \%S) \qquad (6.2)$$

The higher heating value (HHV) was determined using an automatic adiabatic bomb calorimeter (Model No.RSB3, Rajdhani Scientific Instts.Co. New Delhi, India). The FTIR spectroscopic analysis was carried out in the wave number range of 400 to 4000cm^{-1} using an INCOLET FTIR spectroscope (5700 FTIR, Thermo-electron Cooperation Waltham, Massachusetts, USA). The biochemical analysis (hemicellulose, cellulose and lignin contents) was carried out by employing the method of Van Soest (Soest et al., 1991) and (Bledzki et al., 2010).

6.5 Pyrolysis experiments

For pyrolysis experiments a lab-scale experimental setup shown in Fig.6.1 was used. It is essentially a fixed-bed stainless steel tubular reactor (length: 520 mm; I.D. 44 mm) mounted inside an electrically heated vertical tube furnace. Approximately 20g of accurately weighed sample was taken in each run. A constant flow of nitrogen gas (100mL/min) was maintained throughout the experiments to provide inert atmosphere and act as the carrier gas. The condensable vapors were collected in a bottle placed in an ice-bath. After attaining the set temperature, the heating was continued for additional 30min to collect all the condensable as liquid (bio-oil) and complete the char formation. The pyrolysis experiments were carried out in triplicate and average values (standard deviation

of ± 1.0 %) are reported. The yields of pyrolysis product (bio-oil, gas and bio-char) were calculated using the formula:

$$Bio-oil\ \ Yield\ (wt\ \%) = \frac{Bio\ oil\ (g)}{Biomass\ fed\ (g)} X100 \quad (6.3)$$

$$Biochar\ Yield\ (wt\ \%) = \frac{Bio\ char\ (g)}{Biomass\ fed\ (g)} X100 \quad (6.4)$$

$$Gas\ Yield\ (wt\ \%) = 100 - \{Bio-oil\ yield\ (wt\ \%) + Biochar\ yield\ (wt\ \%)\} \quad (6.5)$$

$$Conversion\ (\%) = 100 - \{Biochar\ yield\ (wt\ \%)\} \quad (6.6)$$

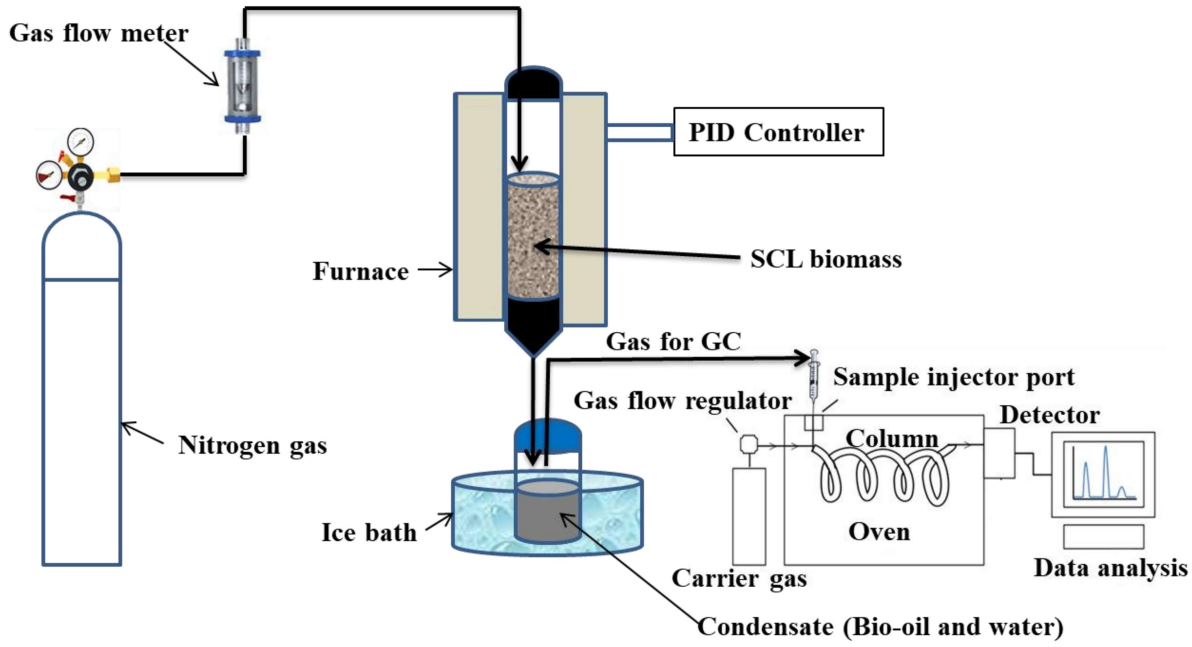

Fig.6.1 Schematic diagram of experimental set-up

6.6 Pyrolysis product characterization

The proximate and ultimate analyses of the bio-oil biochar were performed as per the ASTM standards. The calorific values (MJ/kg) of the bio-oil and bio-char were evaluated using the digital bomb calorimeter mentioned earlier. The FTIR spectroscopic analyses were carried out using a FTIR spectroscope (5700 FTIR, Thermo-electron Cooperation Waltham, Massachusetts, United States) to know the functional groups of chemical compounds present in raw PS biomass and pyrolysis products. The NMR spectroscopic analysis of the bio-oil was carried out using a high resolution nuclear magnetic resonance spectrometer (Burker Bio Spin International AG, Model: AVH D 500 AVANCE III HD 500 MHz One Bay NMR Spectrometer, Billerica, Massachusetts, United States). The solvent for NMR analysis was deuterated dimethyl sulfoxide. The molecular characterization of the bio-oil was carried out using a gas chromatography–mass spectrometry unit (Shimadzu-QP201, Kyoto Japan) equipped with Rxi-5 Sil MS column (30m×0.25mm×0.25μm film thickness) to know the presence of various organic compounds. The compositional analysis of non-condensable gases was performed by gas chromatography (GC) (NUCON 5765) using thermal conductivity detector (TCD) and flame ionization detector (FID) with PORAPAK-Q stainless steel column of dimension (2m × 2mm). Nitrogen was used as the carrier gas with the flow rate of 25mL/min. The oven temperatures were maintained at 110^{o}C and 70^{o}C for TCD and FID whereas the injector and detector temperature for TCD were at 110^{o}C and 120^{o}C and at 70^{o}C and 80^{o}C for FID. 0.1 mL of gas sample was injected for the quantitative analysis using Hamilton-Bonaduz-Schweiz gastight syringe.

6.7. Results and discussion

6.7.1. Particle size distribution and bulk density

A significant parameter influencing thermal conversion is the size of biomass particles. Less time is needed for thermal conversion of small particles (Chen et al., 2017). Char yield reduces, but as the particle size decreases, gas and tar yields grow (Atreya et al., 2017). High heat transfer efficiency and better thermal conversion are allowed by smaller biomass particle size. In the present work all the characterization experiments using SCL biomass particles size in the range of 0.300-0.180mm. The bulk density increases as expected as the particle size decreases in the order of > 0.710mm, 0.710-0.425mm, 0.425-0.300mm, 0.300-0.180mm, < 0.180mm (Fig. 6.2). The pyrolysis process and thermal degradation of a biomass sample are affected by bulk density. In the pyrolysis experiment for bio-oil yield these are the fractions of particle size have been used in this work.

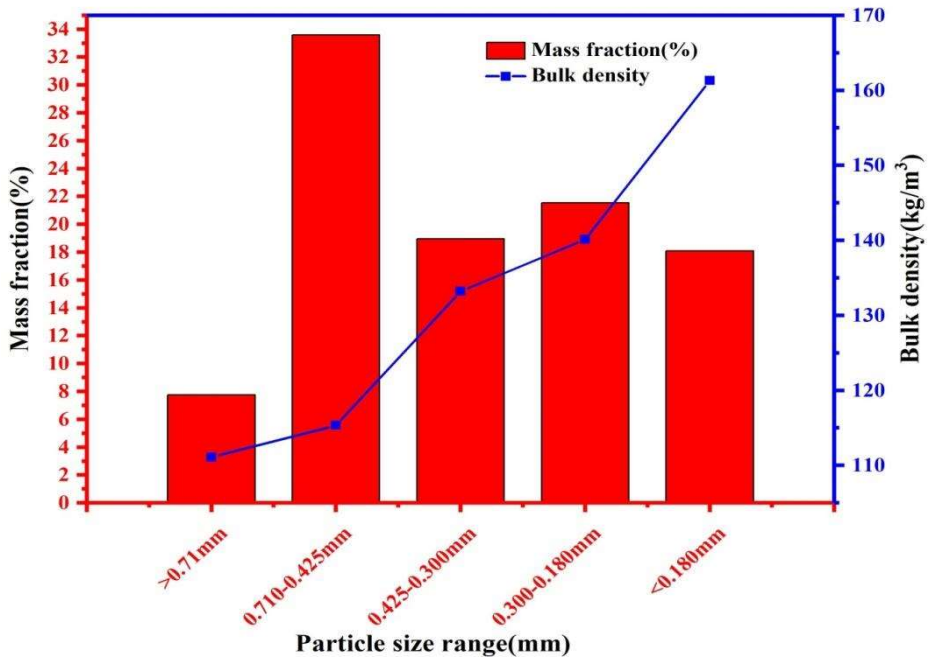

Fig. 6.2 Particle size and bulk density distribution of sugar cane leaves powder

6.7.2. Thermochemical properties

The compositional, proximate and ultimate analyses of SCL performed as per standard protocol indicated that it has 44% cellulose, 42% hemicellulose and 17% lignin contents; 5.67% moisture (MC), 77.33% volatile matter (VM), 10.67% fixed carbon (FC) and 6.38% ash content. Its percentage carbon (C), hydrogen (H), nitrogen (N), and oxygen (O) contents were found as 76.83, 8.19, 0.59, and 14.39, respectively. No sulphur was detected and its calorific value (HCV) was found as 18.08 MJ/kg. The comparison of characteristics of SCL with published similar data for other biomasses indicate that it has the lowest moisture and ash contents compared to sorghum bagasse (MC = 7.60, Ash = 9.50) (Cardoso et al., 2011), corn straw (MC = 6.57, Ash = 11.80) (Gai et al., 2013), rice husk (MC =7.32, Ash = 22.02) (Hu et al., 2016) and *T. latifolia* (Ash = 8.80) (Ahmad et al., 2017). Its volatile matter (VM = 77.33) is slightly lower than that of sorghum bagasse (VM = 81.0) but higher than that of corn straw (VM = 75.00), rice husk (VM = 58.45), and *T. latifolia* (VM = 71.0). The hemicellulose content is nearly similar to that of sorghum bagasse (24%) and corn straw (22.6%); the cellulose content is the highest compared to sorghum bagasse (41%) and corn straw (36.4%). The lignin content the highest compared to these two biomasses. Its calorific value is comparable to that of sorghum bagasse (19.33 MJ/kg) and *T. latifolia* (18.32 MJ/kg).

Biomass having higher VM and low MC, has high calorific value and better ignition and combustion rate (Balasundram et al., 2017; Mishra and Mohanty, 2018). Lower ash content is desirable for reduced aggregation and avoid disposal problems (Müsellim et al., 2018). Thus it can be inferred that the sugar cane leaves are a good feedstock for combustion and pyrolysis.

6.7.3 TG and DTG analyses

Thermogravimetric (TG) and differential thermogravimetric (DTG) analyses provide information and relevant data about the thermal degradation behaviour of biomass and are widely used for the investigating their thermal conversion behaviour. For a typical biomass comprising hemicellulose, cellulose and lignin TG and DTG analyses data are used to obtain kinetic parameters of the overall pyrolysis process as well as the overall order of degradation reaction. In this work TG and DTG analyses of SCL powder were carried out at six different heating rates of 5, 10, 15, 20, 30 and 40^{o}C/min. The data thus generated are shown as percent weight loss and rate of percent weight loss versus temperature plots in Fig. 6.3. From Fig. 6.3, It is clear that the TG versus temperature curves exhibit three distinct zones of weight losses- Zone I (from room temperature 30^{o}C to about 200^{o}C) in which the change in weight of the sample with temperature is very small (around 2 to 5%), Zone II (starting from around 220-250^{o}C and continuing up to about 400^{o}C) in which the maximum weight loss (around70%) is observed and, Zone III (from around 400 till 580^{o}C) in which the percent weight loss is once again low but higher than that observed in Zone I. The weight loss in Zone I is attributed to the loss of inherent moisture (surface moisture and moisture trapped within the intercellular space) and some highly volatile substances. The large weight loss observed in Zone II is primarily due to the thermal degradation of hemicellulose and cellulose molecules. In Zone III volatile complex organic compounds formed through pyrolysis of cellulose and hemicellulose and lignin molecules degrade. Due to their large molecular size and complex nature, the thermal degradation process slows down resulting in much lower percent weight loss compared to Zone II. At the flag end of Zone III, there is hardly any change in the percent weight loss indicating complete

conversion of the biomass to char. Table 6.1 shows TGA and DTG results for the six heating rates used in this work.

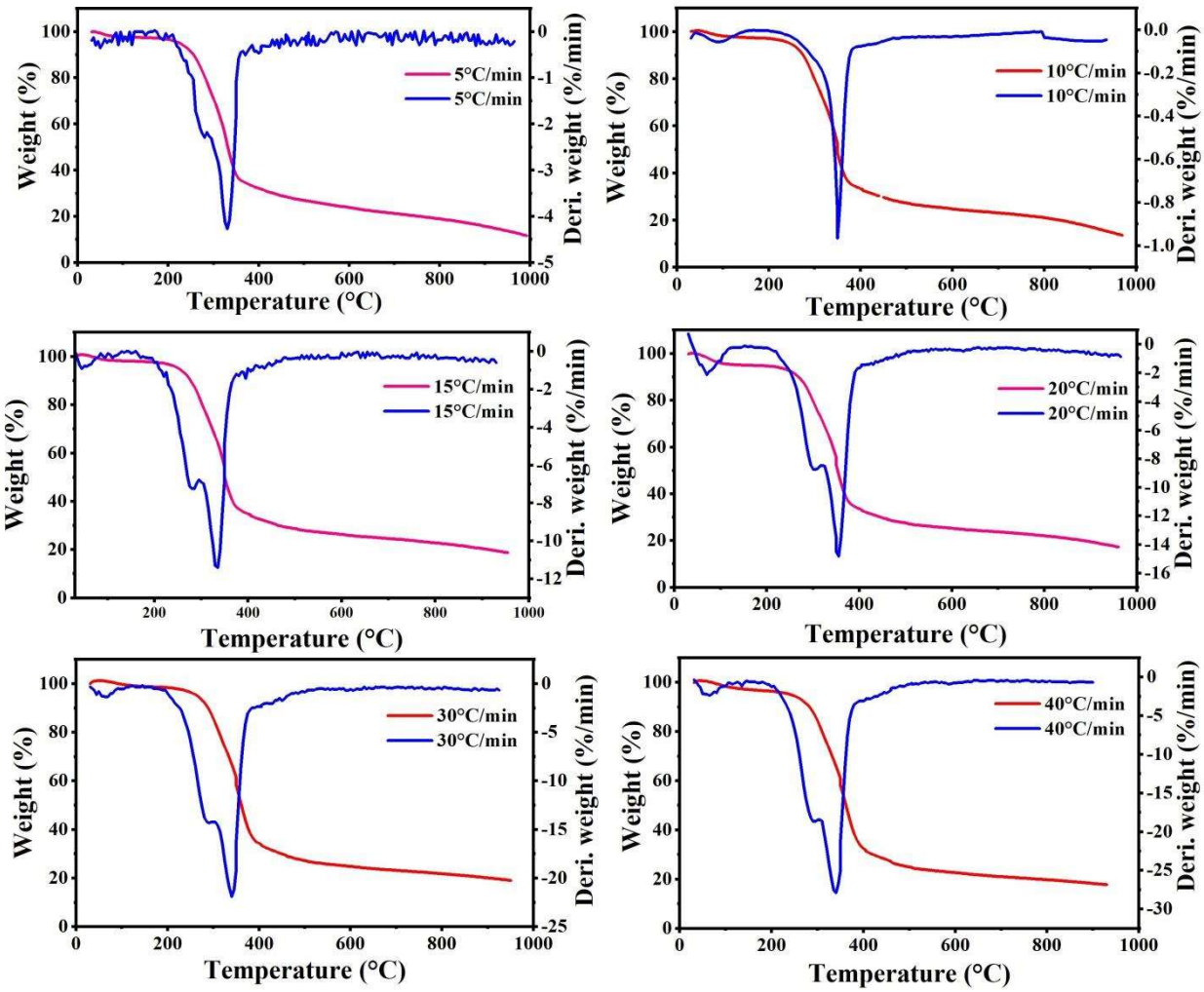

Fig. 6.3 TGA and DTG curves of sugar cane leave powder at different heating rates

6.7.4 Effect of heating rate on TG and DTG analyses

Non-isothermal TG and DTG analyses results for SCL samples are shown in Fig. 1 at different heating rates. The trends of the TGA curves are similar at different heating rates indicating that the overall reaction mechanism is not getting affected by changing the

heating rate (Müsellim et al., 2018). The TG and DTG data obtained at different heating rates are useful for the kinetic analysis of the pyrolysis process. From Fig.6.2 and Table 6.1, it is observed that the temperature decomposition range for each stage increased to a higher range as the heating rate increased from 5 to 40°C/min (Gai et al., 2013). From Table 6.1 it is also seen that the peak temperature of each stage increased with increase in heating rate. The range of active and passive pyrolysis also shifts to higher temperature range as the heating rate increases (Mishra et al., 2015). The residual weight loss increased from 11.74% at 5°C/min to 17.77% at 40°C/min.

Table 6.1: Thermo-gravimetric and differential thermo-gravimetric analyses data of sugarcane leaves at different heating rates

Heating rate, β (°C/min)	Initial Temperature T_i (°C)	Final Temperature T_f (°C)	Peak Temperature T_P (°C)	-DTG_{max}(%/°C)	Weight loss (%)
Stage I					
5	30.09	180	50	0.06	2.75
10	30.20	195	60	0.05	2.92
15	30.34	210	70	0.06	2.50
20	30.14	220	75	0.09	5.56
30	30.33	225	90	0.05	2.16
40	30.25	230	85	0.06	4.33
Stage II					
5	240	500	330	4.27	71.12
10	250	505	340	12.67	71.25
15	255	508	350	11.41	69.79
20	262	515	355	14.82	70.44
30	270	530	360	21.90	72.05
40	280	550	365	27.91	73.84
Stage III					

5	580	992	965	0.05	14.45
10	590	970	915	0.05	12.32
15	600	960	930	0.03	8.96
20	615	965	935	0.02	6.48
30	620	955	915	0.02	6.66
40	630	935	925	0.04	3.98

6.7.5 DSC analysis

Figure 6.4(a) and (b) show the results of DSC as heat flow (mW) versus temperature plots for the heating rates of 5, 15 and 20^{o}C/min and 10, 30 and 40^{o}C/min, respectively. It is seen that the curves have a non-linear nature. In all cases there is an initial portion showing a low peak at 100^{o}C that can be attributed to the evaporation of the inherent moisture. Beyond this there is a slow decline in the heat flow rate up to 400^{o}C and the curves for all heating rates are drooping towards the temperature axis. This can be attributed to the initiation of the pyrolysis reactions which are exothermic in nature. After this temperature the heat flow at all heating rates is increasing steadily with temperature exhibiting the rising trend of curves. The rate of increase is highest for the heating rate of 5^{o}C/min indicating steady progress of the thermal degradation reactions.

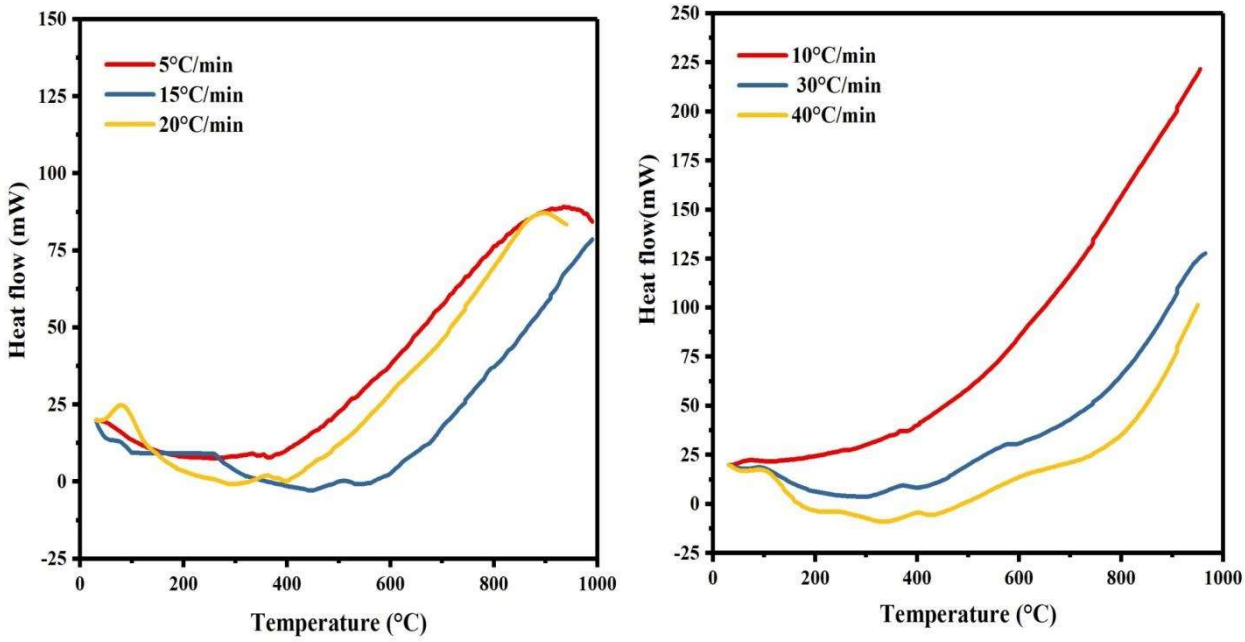

Fig. 6.4 DSC curves of sugar cane leaves powder at different heating rates

6.7.6 Kinetic analysis of thermo-gravimetric results

6.7.6.1 Model-free methods

For designing biomass pyrolyser knowledge of conversion rate, activation energy and pre-exponential factor is crucial. These three kinetic parameters for all six heating rates were calculated using various iso-conversional model-free kinetic methods approved by the Kinetics Committee of the International Confederation for Thermal Analysis and Calorimetry (ICTAC) (Vyazovkin et al., 2011) and as well as the linear regression method (see Table 4.1). In all seven model-free methods were used to evaluate kinetic parameters in the temperature range of 100-600°C. Below 100°C, only water molecules evaporate and above 600°C mainly decomposition of lignin takes place, hence weight reduction data of these ranges have not been considered in the analysis. For analysis the fractional conversion values were taken in the range of 0.05 to 0.95. Biomass pyrolysis involves

several complex heterogeneous reactions taking place in parallel and/or sequence. The rates of these reactions are controlled by the activation energy, the pre-exponential factor and relevant thermodynamic parameters. Values of activation energy and pre-exponential factors were obtained from the slopes and intercepts of linear plots prepared using various model-free iso-conversional methods. Figures 6.5 shows the iso-conversional plots for, FWO, Friedman, Tang, Starink, and KAS models for the conversion(α) range of 0.05 to 0.95. The slopes of the straight lines shown in these figures give the values of activation energy for respective models at various conversions (α) levels. These are listed in Table 6.2 together with the average activation energy values for each model calculated for the entire pyrolysis process. The average values of E for various models range from 214.9 to 239.6kJ $mol^{-1}$and are comparable to those reported for camel grass (E= 84-193 kJ mol^{-1} , β = 10, 30, 50°C/min) (Mehmood et al. 2017), *Typha latifera* (E= 134-204 kJ mol^{-1} , β = 10, 30, 50°C/min) (Ahmad et al. 2017), pea waste (E= 184.4-311.8 kJ mol^{-1} , β = 10, 20, 30, 40°C/min) (Mussellim et al. 2018),*Prosopis juliflora* (E= 164.6-219.3 kJ mol^{-1} , β = 2, 5, 10, 15, 20, 25°C/min) (Chandrasekaran et al. 2017), pinewood (E= 134.3-155.8 kJ mol^{-1} , β = 5, 10, 15, 20, 30, 40°C/min) (Mishra et al. 2015), rice husk (E= 221-229 kJ mol^{-1} , β = 10, 20, 30°C/min) and elephant grass ((E= 218-227 kJ mol^{-1}, β = 10, 20, 30°C/min) (Braga et al. 2014). Among all the model-free methods used in this work the Friedman method gives the highest activation energy. This is more efficient method for pyrolysis kinetic analysis because its rate law is in the differential form and it does not utilise any approximation to estimate the activation energy using TGA data. However, as seen from Fig. 6.6, the numerical differentiation of conversion (α) versus temperature plots required by this method leads to fluctuating activation energy values and low correlation coefficient

(R^2). It is seen that the KAS, FWO, Tang, and Starink models give overlapping plots of activation energy versus conversion with correlation coefficients (R^2) greater than 0.98 indicating a good fit to the experimental data. Vyazovkin model utilises Senum and Yang (Senum and Yang, 1977) approximation for temperature integral which yields insignificant errors. Therefore it can be used very efficiently for the kinetic analysis. Vyazovkin model produces the lowest activation energy among all the models and Vyazovkin AIC model gives values very close to it. This model is an advanced version of the Vyazovkin model and is capable of increasing the accuracy of Vyazovkin model by taking smaller values of $\Delta\alpha$. For solving the temperature integral by the Vyazovkin AIC model, trapezoidal rule has been used. Hence, it can be inferred that the Vyazovkin AIC model produces the most accurate activation energy values. The change in activation energy with changing conversion can be attributed to the difference in the rates of various processes such as loss of moisture, degradation of cellulose and hemicellulose and lignin that take place at different rates during the three stages of thermal degradation. Further, the thermal conversion of the bulk organic fractions of the biomass is also a temperature dependent phenomenon.

Table 6.2: Calculated and average activation energy values obtained from various kinetic models at different values of $\alpha = 0.05 – 0.95$

Conversion(α)	Kinetic methods						
	Vyazovkin	V.AIC	Friedman	FWO	KAS	Starink	Tang
0.05	187.00	193.00	372.74	165.21	169.58	169.61	169.55
0.10	200.00	163.00	225.45	183.96	186.82	186.93	186.89
0.15	81.00	179.00	178.46	168.99	167.17	167.46	167.48
0.20	195.00	153.00	235.29	198.45	199.36	199.58	199.56
0.25	231.00	182.00	284.60	233.25	235.83	236.03	235.99
0.30	198.00	174.00	110.78	201.96	202.80	203.02	203.01

0.35	213.00	184.00	212.74	216.73	218.17	218.38	218.36
0.40	209.00	167.00	235.49	212.77	213.93	214.15	214.13
0.45	201.00	237.00	306.57	197.48	197.72	197.96	197.96
0.50	220.00	163.00	193.89	223.33	224.76	224.98	224.97
0.55	224.00	179.00	210.87	227.41	228.99	229.22	229.19
0.60	206.00	222.00	210.97	210.94	211.55	211.79	211.78
0.65	210.00	222.00	87.50	214.30	215.00	215.25	215.24
0.70	213.00	230.00	329.10	217.89	218.68	218.92	218.91
0.75	217.00	229.00	370.48	221.24	222.123	222.37	222.36
0.80	183.00	150.00	450.34	188.91	187.10	188.27	188.29
0.85	266.00	272.00	218.79	271.88	275.89	276.07	276.02
0.90	607.00	434.00	88.62	392.54	405.95	405.90	405.72
0.95	26.00	350.00	229.25	365.20	325.95	326.05	325.95
Avg.	**215.11**	**214.89**	**239.58**	**226.97**	**226.75**	**226.94**	**226.91**

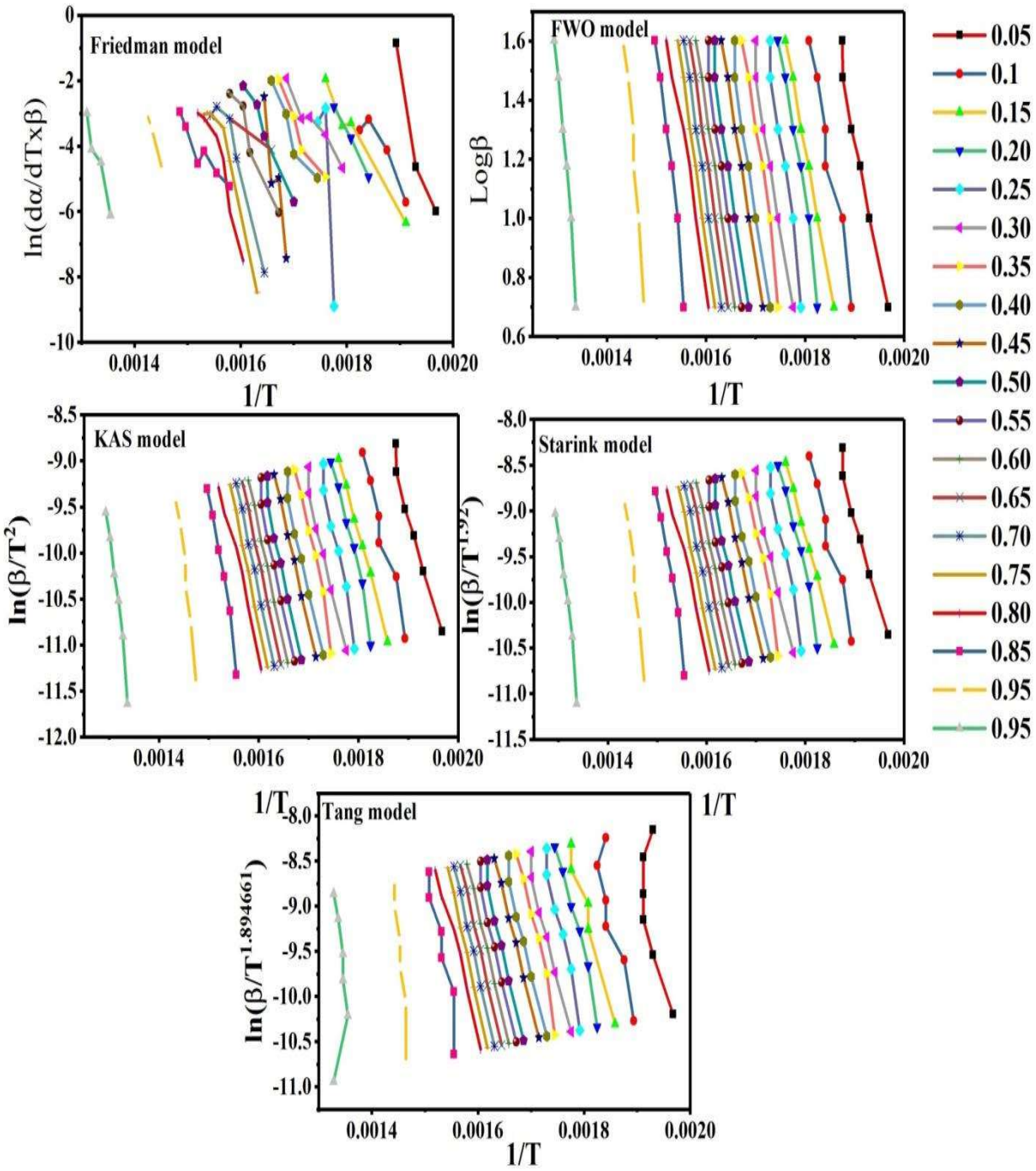

Fig. 6.5 Kinetic plot for sugarcane leaves under nitrogen environment using various model

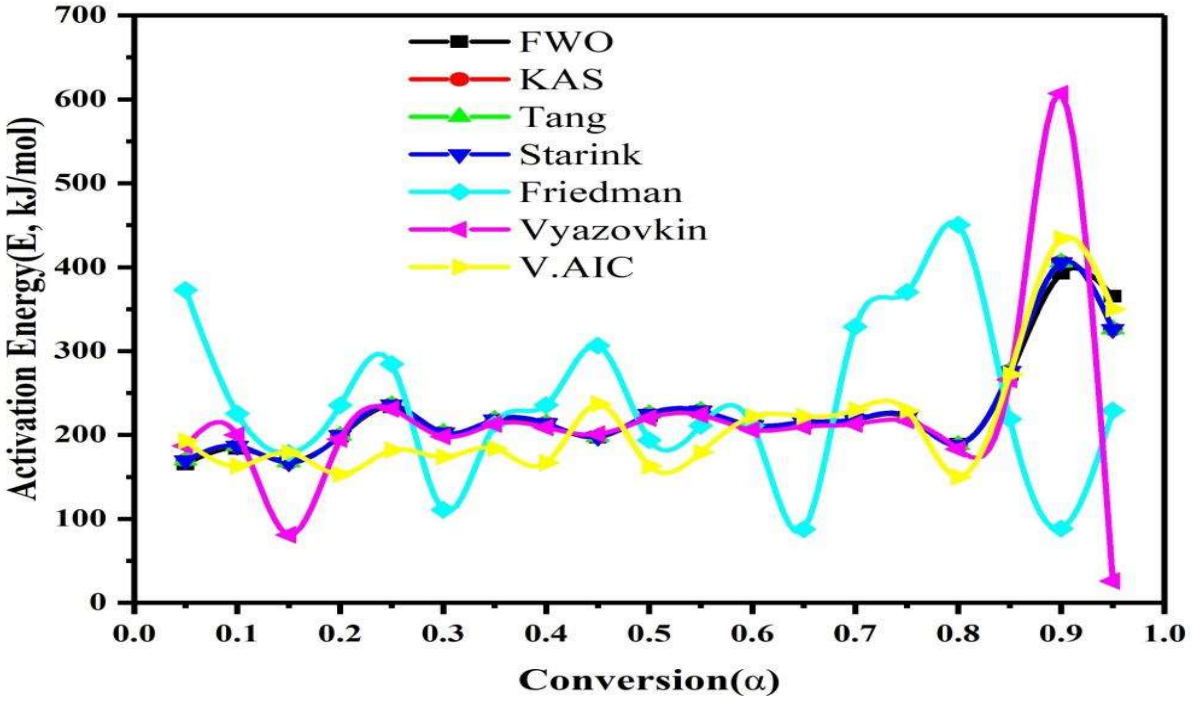

Fig. 6.6 Variation of activation energy with conversion using different kinetic models

6.7.6.2 Multiple linear regression method

The multiple linear regression analysis was also used for analysing TGA data. The coefficients B, C, and D of the multiple linear regression method represent ln (A), activation energy, E, and the order of reaction, n, respectively. Unlike other models, this method cannot give the values of these coefficients for every conversion of the pyrolysis process.

Through this method, the activation energy values were obtained in the range of 25.06 to 57.23kJ/mol and the pre-exponential factor in the range of 5.20 to 2.8×10^4 min^{-1} at various heating rates. The order of reaction varied between 1.04 and 1.41 indicating approximately a first order reaction throughout the pyrolysis process. Similar results were also reported by Kumar et al. (2008), Mansaray and Ghaly (2015) and Yin and Goh (2015) . Here also it is

seen that the activation energy and pre-exponential factor increase as the heating rate increases slightly because the pyrolysis process is affected more due to increase in heating rate rather than the kinetic triplet.

6.7.7 Prediction of reaction mechanism

It is difficult to come out with a reaction mechanism for complex reactions occurring in parallel and series during pyrolysis of a complex material like biomass. However, efforts have been made to come out with the help of appropriate mechanistic model based mathematical relations. Here the Criado method (Criado et al., 1989) has been used to evaluate the reaction mechanism of SCL biomass pyrolysis. In this method experimental and theoretical z (α) versus conversion curves are compared. The theoretical curves were obtained from Eq. (4.54) for f (α) and g (α) functions applicable for different mechanism and are known as master curves (Table 4.2). The experimental z (α) curve was obtained using the activation energy value obtained from Vyazovkin AIC and heating rate (β) at 5^{o}C/min using Eq. (4.56) because of the reasons mentioned earlier.

Figure 6.7 compares the experimental and theoretical z (α) curves for various mechanisms. It is refer that below the conversion value 0.2, the experimental z (α) is overlapping with the A_3 master curve and is close to the A_2 and A_4 master curves. According to Avrami, these master curves are valid for the nucleation and growth mechanisms. For the conversion range of 0.3 to 0.8, the experimental curve is lying in between A_2 and A_3 master curves, indicating once again the validity of nucleation and growth mechanism. Similar results were obtained by Dhyani et al. (2017) for sorghum straw pyrolysis. For the conversion between 0.80-0.95, the experimental curve is close to F_1 and F_2 master curves

indicating the validity of the mechanism of random nucleation with one nucleus on the individual particles. This observation is similar to the observation of Poletto et al (2012) for wood pyrolysis. Based on these observations it is possible to infer that the degradation initiates from random points acting as growth centres for the propagation of degradation reactions. After the removal of inherent moisture, the degradation of biomass will proceed through the rupture of bonds of long chain cellulose and hemicellulose molecules resulting in low molecular weight (or smaller chain molecules) that act as sites for random nucleation and growth. The cellulosic and hemicellulose components of SCL are predominantly amorphous that may cause better transfer of heat to the interior of the particles resulting in the formation of nucleation sites for promoting the thermal degradation.

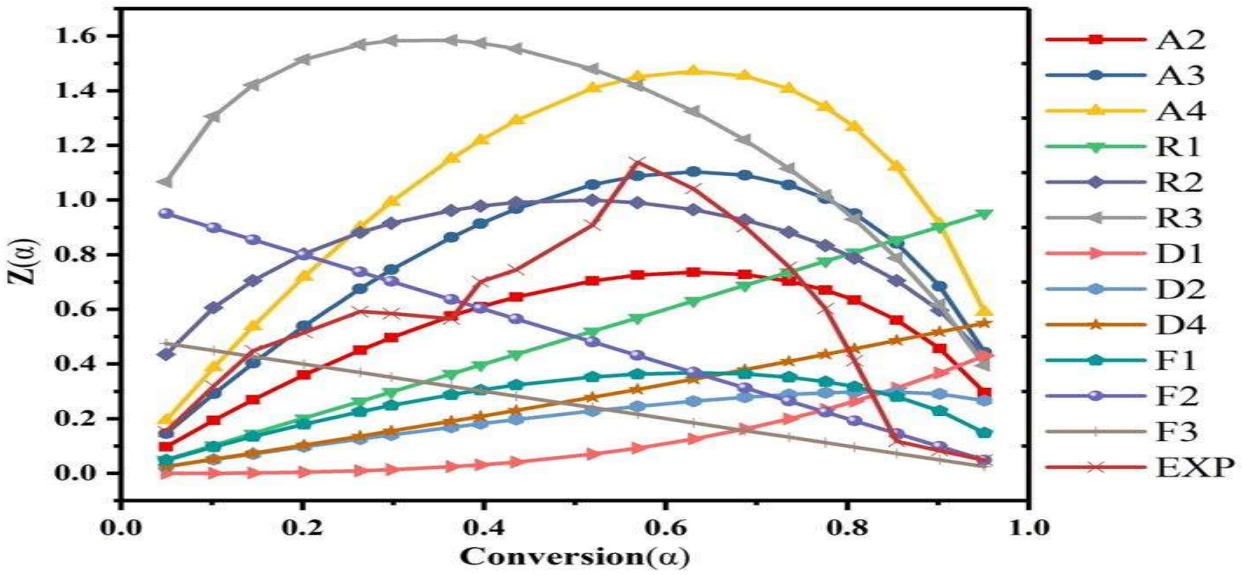

Fig. 6.7 z(α) master plots for sugar cane leaves using Criado method (Criado al., 1989): Nucleation and growth based mechanisms (A2, A3, & A4); Phase boundary-controlled reaction (R1 – one dimensional movement, R2 – contracting area, R3 – contracting volume); Diffusion based models (D1 – one-dimensional,D2 – two dimensional, D4 – three dimensional); Random nucleation site based models (F1 – one nucleus on individual particle, F2 – two nuclei on individual particle, F3 – three nuclei on individual particle.

6.7.8 Pyrolysis and product distribution of SCL

Pyrolysis of SCL has been performed using lab scale fixed bed reactor by varying various parameter such as process temperature, heating rate, particle size of feedstock and bed height of the sample in the reactor. The pyrolysis product distributions of SCL with various operational parameters are depicted in Fig. 6.8(a)-(d) and are presented in Table 6.3. These parameter are strongly influences the product yield (liquid (bio-oil), non-condensable gas and solid product). Previously various workers have been performed pyrolysis experiment using different feedstocks with varying these parameters such as teak sawdust (Gupta et al., 2019), neem seed (Mishra et al., 2018) and sugar cane leaves (Charusiri et al., 2018).

Table 6.3: Product distribution of SCL pyrolysis

Temperature (°C)	Heating rate (°C/min)	Bed height (cm)	Particle size (mm)	Bio-oil (Wt. %)	Biochar (wt. %)	Gas (wt. %)	Conversion (%)
350	25	16	0.300-0.180	36.71	36.82	26.47	63.18
450	25	16	0.300-0.180	41.82	30.64	27.54	69.63
550	25	16	0.300-0.180	43.78	25.02	31.20	74.98
650	25	16	0.300-0.180	39.28	24.05	36.67	75.95
550	15	16	0.300-0.180	34.71	33.82	31.47	66.18
550	20	16	0.300-0.180	42.82	29.64	27.54	70.36
550	25	16	0.300-0.180	44.78	26.02	29.20	73.98
550	30	16	0.300-0.180	37.28	23.05	39.67	76.95
550	25	4	0.300-0.180	34.71	31.62	33.67	68.38
550	25	8	0.300-0.180	37.69	30.14	32.17	69.86
550	25	12	0.300-0.180	40.38	27.32	32.30	72.68
550	25	16	0.300-0.180	42.18	24.15	33.67	75.85
550	25	16	0.300-0.180	41.23	32.16	26.61	67.84
550	25	16	0.425-0.300	39.62	35.63	24.75	64.37

550	25	16	0.710-0.420	38.69	34.26	27.05	65.74
550	25	16	>0.71	37.95	35.12	26.93	64.88

6.7.8.1 Effect of process temperature

Pyrolysis of SCL has been performed at different temperature of 350, 450, 550 and 650ºC. The pyrolysis product distributions with temperatures are illustrated in Fig. 6.8(a). To study the variation of temperature on product yield of SCL pyrolysis, approximately particle size in the range of 0.300-0.180mm, bed height of 16cm and heating rate of 25ºC/min were selected with constant rate of nitrogen flow throughout the experiment. It was observed that as the temperature increases the conversion of feedstock into end product increases (Table 11.1) and similar results were reported by Mishra et al., (2018) and Charusiri et al., (2017). It can be seen from Fig. 6.8(a) that the yield of non-condensable gas increases with increase in processes temperature and this similar phenomenon is previously observed by Mishra et al., 2018 for neem seed pyrolysis. Gas yield was increases from 26.27% to 36.20% as temperature increases from 350ºC to 650ºC. This increase of gas with temperature is mainly due to the rapid thermal degradation of biomass at higher temperature and volatiles were converted in to the non-condensable gases because of rapid endothermic decomposition (secondary reaction). Moreover, the primary degradation of low moisture content biomass or secondary decomposition of the biochar at higher temperature (Charusiri and Numcharoenpinij, 2017). The maximum liquid yield of 44.23% was observed at 550ºC. The yield of bio-oil increases up to the temperature of 550ºC and beyond this temperature it was decreased because of decomposition of biomass. Initially (at 350ºC) the yield of liquid product was low due to the partial decomposition of biomass.

This variation exhibited that the distribution of liquid product is also not steady with temperature as gas yield. Additionally it was also noticed that, beyond 550^{o}C temperature the liquid yield decreased and it may be possibly due to the continuous cracking of the intermediate hydrocarbon compounds from the primary and secondary reactions into a gaseous product. Therefore, it leads to the formation of extra non-condensable gases at higher temperature. The solid product (biochar) decreases with increase in temperature Fig. 6.8(a).This may be attributing to the higher decomposition efficiency (higher heat and mass transfer among biomass particle) and secondary reaction of char into non-condensable gas (Mishra et al., 2018).

6.7.8.2 Effect of heating rate

Heating rate is also an important parameter in order to alter the product yield of biomass pyrolysis (Mishra et al., 2018). The pyrolytic product distributions with heating rate are presented in Fig. 6.8(b). The Heating rate were varies from 15 to 30^{o}C/min (15, 20, 25 and 30^{o}C/min). It was noticed that the yield of bio-oil increases from 34.25% at 15^{o}C/min to 44.23% at 25^{o}C/min and beyond this decreased to 34.12% at 30^{o}C/min. More or less similar trend were also observed by Mishra et al., (2018) for neem seed and Xiong et al., (2018) for rice husk. It was also observed that liquid yield was higher than the biochar at all heating rates and higher than gas also excepting at 30^{o}C/min. The yields of biochar decreases while those of bio-oil increase for the low and medium heating rate. The decrease in the biochar yield could be due to either greater primary decomposition of biomass or through secondary decomposition of the biochar. The non-condensable gas yields increase as temperature increase for medium and high heating rate. It may be possible due to that at higher heating rate produces more volatile compound. At fast

heating rate, the bio-oil sample would be heated to high temperature quickly, causing a large proportion of bio-oil to be evaporated as gas phase volatile in the reactor.

6.7.8.3 Effect of Particle size

The effect of particle size on pyrolytic product distribution is illustrated in Fig 6.8(c). Effect of particle size variation on product yield have been performed with particle size of > 0.71mm, 0.710-0.425mm, 0.425-0.300mm, 0.300-0.180mm at 550^{o}C temperature in presence of constant flow rate of nitrogen gas. Particle size may affect the heat and mass transfer between the feedstock, degradation of biomass, devolatilization to volatile vapors, and the thermal decomposition of tar during the pyrolysis. It can be observed from Fig 6.8(c) that the bio-oil yield decreases slightly with increase in the particle size because of poor heat and mass transfer consequently partial combustion of biomass sample (Mishra et al., 2018). The change in yield of gas was not so affected due to changes in particle size. During pyrolysis, adequate heat transfer to smaller SCL particles with a higher heating rate facilitates the volatilization of SCL into volatile vapors that create more non-condensable gases and therefore less biochar. In addition, as the particle size increases, the pyrolysis of SCL primarily happened on the surface of the biomass sample, and the overall size distribution and uniformity of the biomass sample influenced the heat and mass transfer. The resistance to heat transfer impacted the liquid substance more intensely than an increase in the average particle size because the internal temperature during the primary pyrolysis stage may have been inadequate to finish the thermal degradation process (Luo et al., 2013; Oudenhoven et al., 2015; Moralı et al., 2016; Xu et al., 2017).

6.7.8.4 Effect of bed height

The effect of packed bed height on the production of the pyrolysis product is much less studied previously, but it also has a significant influence on the delivery of the product. Although the heating zone was more or less 16cm in the split tube furnace, there were differences in bed height from 4 to 16cm at the middle of the heating zone. The increase in packed bed height from 4 to 16cm indicating increase in bio-oil yield and a very small decrease in biochar yield pyrolytic non-condensable gas yield as seen in Fig. 6.8(d). This may be because a rise in the height of the packed bed resulted in a longer period of residency in the compact biomass bed and a more secondary cracking reaction. Similar results were also observed by Gupta et al., (2019) for sawdust and Zhang et al. (2009) for corncob pyrolysis.

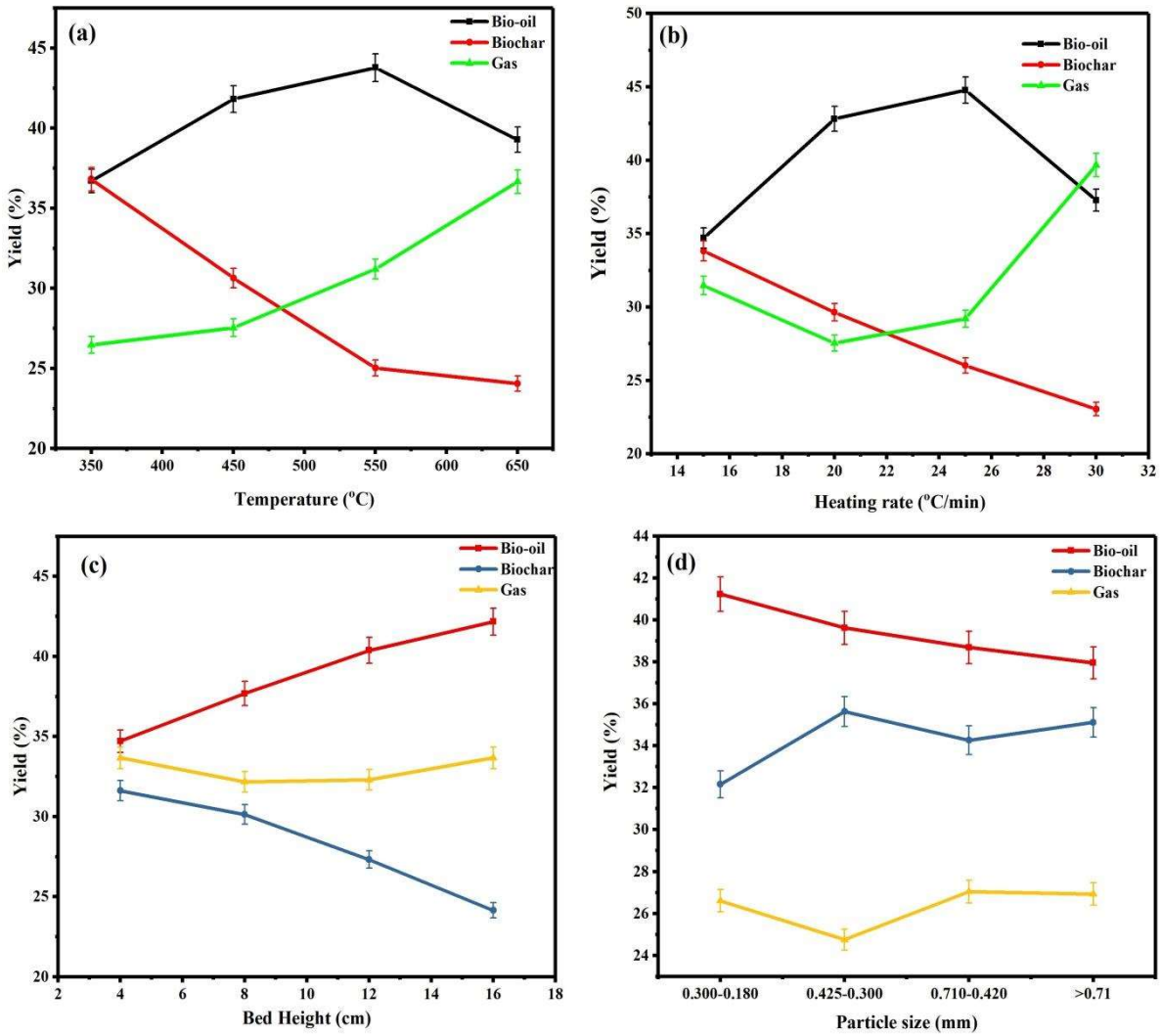

Fig.6.8 Effect of process parameters (a) temperature (b) heating rate (c) packed bed height and (d) particle size

6.7.9 Characterization of pyrolytic liquid product

6.7.9.1 Physicochemical properties of bio-oils

Produced bio-oil contains organic phase as well as aqueous phase. Therefore, collected liquid product from bottom of the condensing unit extracted (liquid- liquid extraction) with dichloromethane (CH_2Cl_2) in order to separate the organic phase and aqueous phase

(Charusiri et al., 2018). Detailed properties of bio-oil (organic phase) produced from pyrolysis of SCL at optimum conditions (temperature- 550^{o}C, heating rate- 25^{o}C/min, bed height- 16cm and Particle size- 0.300-0.180mm) analysed and presented in Table 6.4 with the properties of diesel. Approximately 8 wt. % moisture was estimated in SCL bio-oil where diesel has no moisture. This value of moisture content is lower than those reported for other bio-oils obtained from other biomass such as sugarcane, which is in the range of 15% to 30% (Zhang et al., 2007) and similar results were reported by David et al., (2018) and Charusiri et al., (2018). From ultimate analysis of bio-oil it was observed that the carbon content in bio-oil is less than the raw SCL sample. It also revealed that the H/C and O/C values are lower than SCL raw sample. It is may be due to that, during pyrolysis a condensable bio-oil product formed, and CO and CO_2 were removed as non-condensable gas from the biomass feedstock(Charusiri et al., 2018). The appearance of moisture content in the bio-oil sample reduces the temperature of ignition of combustible bio-fuel, but on the other hand it decreases the viscosity and as a consequence increases the fluidity. Then again, the moisture in the bio-oil advances an incomplete ignition and improves the evolution of smoke, whereby the ignition temperature what's more, the generation of heat is diminished. Combustion rate also reduces and combined with these progressions it is the impact of water in diminishing radiant outflow from the flam. As a result, the mixture of these effects results in major variations in the flames characteristics of moisture-containing fuels (David et al., 2018).The bio-oil is acidic in nature because the pH was found to be 2.12. The acidity of bio-oil is mainly due to the presence of carboxylic acids, phenolic compounds, and their derivatives (Kumar et al., 2009). The acid number was estimated by titration method using N, N-dimethyl formaldehyde and methanol as the solvent. It was

found to be 28mgKOH/g and this is close agreement with other published result (Charusiri et al., 2018). This indicates the corrosive nature of bio-oil. The density of bio-oil was estimated to be 1089kg/m^3 is more than diesel due to the presence of oxygenated heavy organic compounds such as phenols (Gupta et al., 2019) and similar results were reported by Verma et al., (2019). The Ramsbottom carbon residue (RCR), the carbon forming property of the oil at high temperatures is 2.89wt. %. The ash content the bio-oil is estimated to be 0.06 wt. % which is in the acceptable range. The higher heating value was found to be 27.39 MJ/kg, indicating the bio-oil to be a good fuel. The empirical formula and HHV are reported in Table 6.4and these are matching with previously reported data (Verma et al., 2019).

Table 6.4: Physicochemical properties of bio-oil sample

Properties	Bio-oil	Diesel
Ultimate analysis (wt %)		
C	52.23	86.50
H	8.29	13.20
N	0.56	0.00
O	38.92	0.00
S	-	0.30
H/C	1.90	1.83
O/C	0.55	0.00
N/C	0.009	0.00
Empirical formula	$CH_{1.90}O_{0.55}N_{0.009}$	$CH_{1.83}\ S_{0.0013}$
Appearance	Dark brown	-
Moisture content (wt %)	~8.26	0.00
pH	2.12	-
Acidity(mg_{KOH}/g)	28	-
Density(kg/m^3)	1089	820
Kinetic viscosity (pa-s)	0.69	-
Ramsbottom carbon residue (wt. %)	2.89	-
HHV (MJ/kg)	27.39	-

Ash Content (wt. %)	0.06	0.00

6.7.9.2 FTIR analysis of bio-oil

FTIR spectra have been used to identify the major functional group and their derivatives such as C-H, O-H, C=O, C=C and C-O present in the bio-oil sample (Fig. 6.9). A wider peak in the range of 3400 and 3500cm^{-1} is due to the O-H group of phenols and alcohols (Rout et al., 2016). A peak at around 3000cm^{-1} is dedicated to C-H stretching of alkanes and alkenes in bio-oil (Capunitan and Capareda, 2012). Peaks observed in between 1600 and 1500cm^{-1} in bio-oil sample represent the C=O stretching of carbonyl group. These indicate the existence of aldehydes, ketones and carboxylic acids (Demiral and Kul, 2014). Large number of small peaks in between 1000 and 1500cm^{-1} are due to the presence of C-O stretch of ethers and esters in bio-oil (Abnisa et al., 2013; Capunitan and Capareda, 2012). C-H vibrations of alkenes in the range of 610–620cm^{-1} observed (Abnisa et al., 2013). Therefore it can be conclude that the bio-oil is mixture of valuable organic compounds which may be usable as liquid fuel after upgrading or as source of valuable chemicals. The detailed information of bio-oil component was found by using GC-MS analysis.

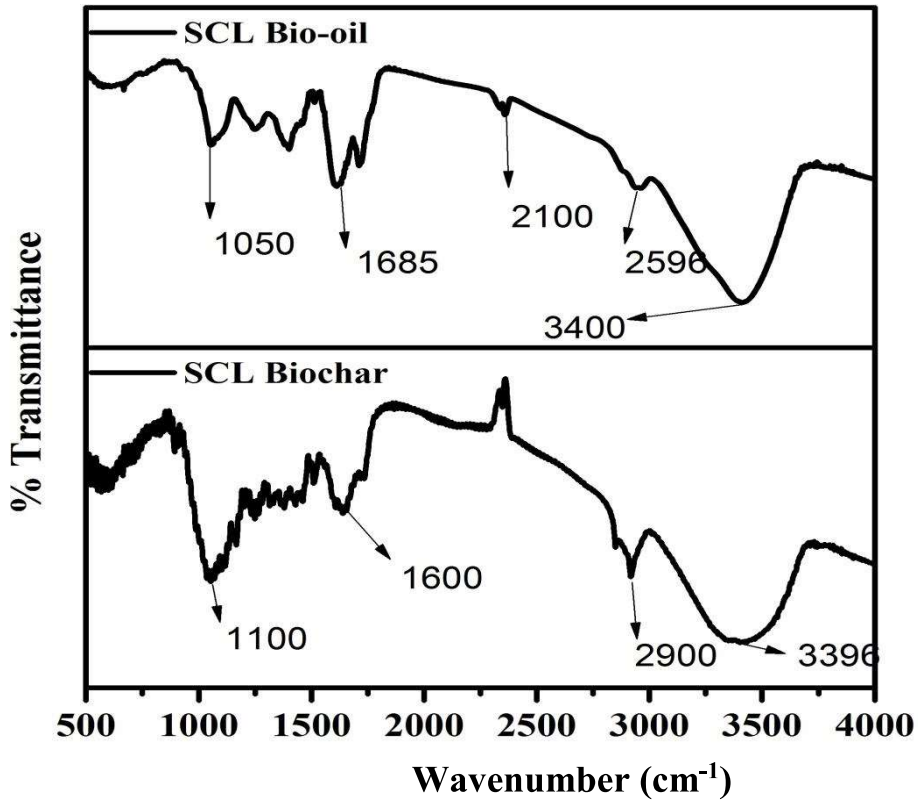

Fig. 6.9 FTIR spectra of bio-oil and biochar sample

6.7.9.3 GCMS analysis of bio-oil

GCMS analysis of bio-oil sample has been performed in order to detailed component present in the sample. For this purpose the bio-oil sample was first diluted with hexane. The chromatographic diagram indicates more than 100 peaks and the components were identified by using the National Institute of Standards and Technology (NIST) library. The major identified compounds are presented in Table 6.5. These compounds observed were mainly due to the degradation of SCL component (cellulose, hemicellulose and lignin). As per the FTIR analysis bio-oil is a mixture of branched or stretched chain organic compounds which mainly containing aldehydes, phenol, ketones, and ester related compounds and also some oxygenated organic compounds. Benzene, phenols and their derivatives were obtained due to the thermal degradation of lignocellulosic SCL (cellulose,

hemicellulose and lignin).The major phenolic and other compounds include phenol, 2,6-dimethoxy-, Decane, creosol, phenol 4-ethyl-2-methoxy-, 2-furanmethanol, 2-cyclopenten-1-one, 2-Cyclopenten-1-one, 2-methyl-, Phenol, 4-(2-propenyl)-2,6-dimethoxy-, 3-Methylcyclopentane-1,2-dione, 3-methyl-, 2-methyl-3-hexanone, 2-cyclopenten-1-one, 3-ethyl-2-hydroxy-,(E)-9-Octadecenoic acid ethyl ester, phenol, 2,6-dimethoxy-, 5-methyl-1,3-benzenediol, phenol, 2-methoxy-4-(1-propenyl)-, and 2-propanone, Ethyl 9-hexadecenoate and are due to the decomposition of lignin. Acidic compounds and their derivative such as acetic acid butanoic (or butyric) acid, etc. are formed mainly due to the decomposition of hemicellulose (Biswas et al., 2017). The nitrogenous compounds like pyridine, 2-ethyl-, N-(n-butoxymethyl) acrylamide, pyridine 2, 5-dimethyl- etc. present in the bio-oil may be attributed to the protein based compounds of raw SCL sample.

Table 6.5: GC–MS analysis of bio-oil

R.Time	Area%	Name
6.448	7.89	2-Furanmethanol
6.521	9.56	Phenol, 2,6-dimethoxy
6.628	3.32	2-(Acetyloxy) Ethyl acetate
6.990	0.32	1,6,6-Trideuterocyclohexa-2-EN-1-OL
7.260	2.15	2-Cyclopenten-1-one, 2-methyl-
7.393	1.11	Ethanone, 1-(2-furanyl)-
7.498	0.61	Silane, phenyl-
7.864	1.70	N-(n-Butoxymethyl) acrylamide
7.882	3.02	Benzene, 1,2,4,5-tetrafluoro-3-methoxy-
8.675	5.24	Phenol, 4-(2-propenyl)-2,6-dimethoxy-
9.308	0.27	2(5H)-Furanone, 3-methyl-
9.500	0.16	Decane
9.628	0.28	2-Furan methanol, Acetate

9.923	2.62	3,5-Dimethoxy-4-hydroxyphenylacetic acid
10.871	3.92	3-Methylcyclopentane-1,2-dione
11.258	0.27	Oxazole, 2-ethyl-4,5-dihydro-
11.960	1.70	2-Furaldehyde diethyl acetal
12.158	0.48	2-Octen-4-ol
12.514	10.56	Phenol, 2-methoxy-
13.340	0.25	Octanoic acid, methyl ester
14.258	0.10	Bicyclo heptane-1,2-dicarboxylic acid
14.361	0.23	2-Pentanone, 5,5-diethoxy-
14.863	0.29	4,4,6-Trimethyl-cyclohex-2-en-1-ol
15.178	0.29	Phenol, 3-Ethyl-
15.497	1.45	Creosol
17.872	1.12	Phenol, 4-ethyl-2-methoxy-
19.916	0.72	Phenol, 2,6-dimethoxy-
21.000	0.12	Decanoic Acid, Ethyl Ester
23.218	0.22	Benzene, 1-(1,5-dimethyl-4-hexenyl)-4-methyl-
26.050	0.17	Hexadecane
30.353	0.19	Ethyl 2-hydroxy-4-methoxy-6-propylbenzoate
33.041	0.17	Hexadecanoic Acid, Methyl Ester
36.524	0.45	9,12-Octadecadienoic acid, methyl ester
37.456	3.06	Linoleic acid ethyl ester
37.540	6.74	(E)-9-Octadecenoic acid ethyl ester
37.857	0.99	Octadecanoic Acid, Ethyl Ester
38.512	0.30	Methyl 9-cis,11-trans-octadecadienoate
38.642	0.57	Cyclopropaneoctanoic acid, 2-hexyl-, methyl ester
38.929	0.19	3,5-Dimethoxy-4-hydroxycinnamaldehyde
39.489	1.58	Ethyl 9-hexadecenoate
40.709	0.26	1,2-Benzenedicarboxylic Acid
40.817	0.23	Octadec-9-Enoic Acid
41.575	0.21	9-Octadecenoic acid (Z)-, 2-hydroxy-1 (hydroxymethyl)ethyl ester

41.783	0.43	Phenol, 2-methoxy-
42.833	0.18	Heptadecanoic Acid, Ethyl Ester

6.7.9.4 ^{1}HNMR analysis of bio-oil

The ^{1}HNMR spectra analysis of the SCL pyrolysis bio-oil sample is important technique in order to get the idea about the approximate ratios of the chemical environment of the proton (Biswas et al., 2017; Mullen et al., 2009). The integral values of the specific peaks are presented in Table 6.6. The results of ^{1}HNMR spectra are stated in terms of peak allocated to their respective functional groups, like FTIR. The protons of the aliphatic and alkyl group carrying molecules are indicated by the unfiled area of ^{1}HNMR (0.5 to 1.5 ppm) spectra. The proton of the allylic group found in carbonyls (ketones, esters, aldehydes, acids, and amides), alkenes or amides, corresponds to the next region (1.8 to 2.8 ppm).The 2.8 to 4.5 ppm spectra refer to protons found in alcohol, ether and ester containing single bonds of oxygen and CH_2 bound to two aromatic rings. Peaks in the 6.5 to 8.5 ppm region correspond to the group of aldehyde protons.

Table 6.6: ^{1}H NMR analysis of bio-oil

Chemical shift (ppm)	Type of hydrogen present
0.5 - 1.5	Proton present in short chain aliphatic group and many molecules with non-functional alkyl portions will give a lot of signal in this area.
1.8 - 2.8	Proton on allylic group and it appears when carbonyls (ketones, esters, aldehydes, acids, and amides), alkenes or aromatics of the double bonded function group are present
2.8 – 4.5	Proton present for alcohol, ethers of esters functional groups that contain oxygen single bonds and CH_2 attached with two aromatic

	rings.
6.5 – 8.5	Protons of aldehyde functionality.

6.7.10 Biochar Characterization

Physicochemical properties (Proximate, ultimate and higher heating values) of biochar are reported in Table 6.7. It can be observed from Table 6.7that the moisture content of biochar decreases as compared to raw SCL after pyrolysis and it is due to the evaporation of moisture. Volatile matter decreased in biochar and found to be 10.45% and on the other hand the fixed carbon increased up to 10.96% as compared to raw SCL. The increment of ash content in biochar is because of removal of volatiles present in raw biomass and accumulation of inorganic elements present (Tag et al., 2016). It is also interesting to mention that the ash content in present biochar is lower than Indian coal which is lies in the range of 25 to 40% (Anupam et al., 2016). Higher ash content is undesirable parameter as it decreases the energy value of the fuel. The ratio of VM/FC decreases to 0.13 from 7.25 (raw SCL) and increase in the HHV (23.46MJ/kg) due to increase in fixed carbon content which indicate superior quality of fuel. It was observed from ultimate analysis that the ratio of H/C of biochar was less than 1.0 and decreasing values of this indicating higher degree of carbonization and increasing fuel value (HHV). Moreover, the carbon content of biochar increases as compare to raw SCL, showing that the biochar need to be purified to obtain activated carbon for additional use.

Table 6.7: Physicochemical properties of biochar sample

Analysis	Biochar sample
Proximate analysis (wt. %)	
Moisture content	1.12
Volatile matter	10.45
Ash content	10.96
Fixed carbon	78.59
VM/FC	0.13
Ultimate analysis (wt. %)/	
C	78.35
H	5.14
N	0.37
S	-
O	16.14
H/C	0.79
O/C	0.15
HHV(MJ/kg)	23.46
ICP AES analysis	
Sodium	3.01
Magnesium	5.19
Aluminum	4.56
Silica	8.37
Potassium	5.63
Calcium	10.23
Manganese	3.13
BET surface area (m^2/g)	235.17

6.7.10.1 XRD analysis of biochar

The study of SCL and its biochar X-ray diffraction pattern is provided in Fig. 6.10. At 2Φ values about 18.5^o and 22.5^o, the intensity and sharpness of the peak indicate the presence of amorphous and crystalline cellulose in SCL. However, compared to SCL, pyrolysis resulted in a total shift in the crystallographic nature of biochar. The peaks in biochar have been reduced during pyrolysis, suggesting cellulose degradation (Wang et al., 2009). In Fig. 6.10, peak observed in biochar sample in the range of 25^o to 30^o belongs to the quartz crystallographic structure. Other investigators have also confirmed the presence of such a peak (He et al., 2018).The crystallographic structure of calcite corresponds to another peak

around at 2Φ = 30^{o} (He et al., 2018). The rise in the sharpness of the peak is attributed to the relative decrease in the amorphous organic process and increase in the ash percentage, as well as the structural changes in the SCL biochar (Zhang et al., 2015; Abrego et al., 2009).

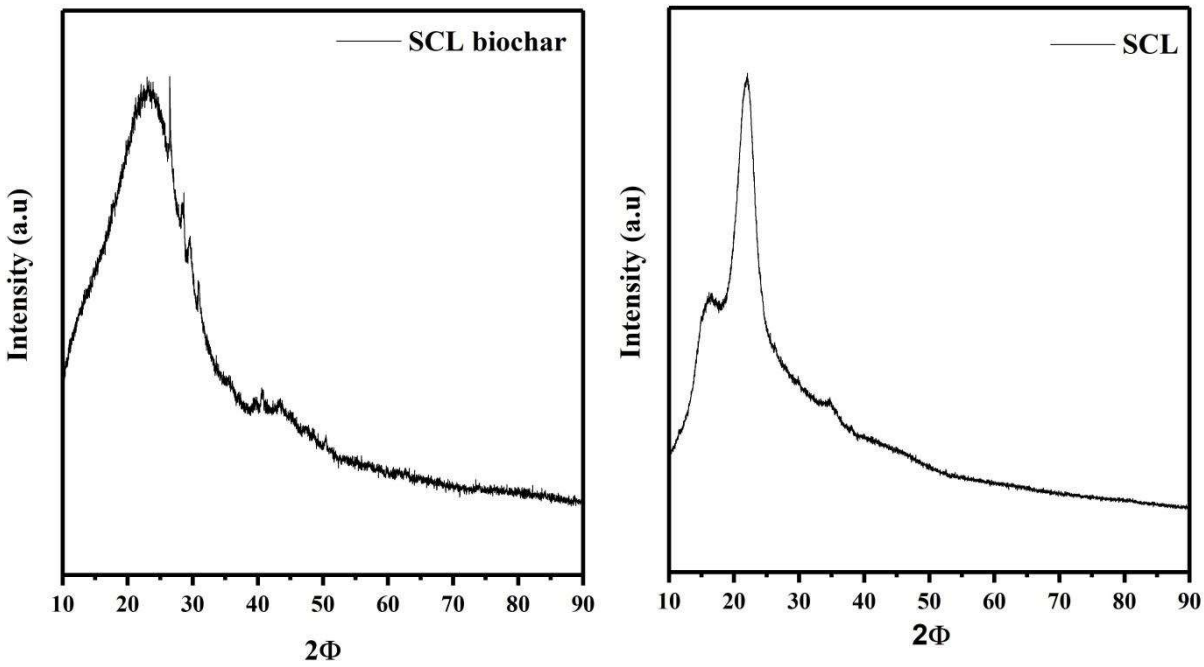

Fig. 6.10 X-ray diffractogram of SCL biochar and SCL

6.7.10.2 SEM and EDX analysis of biochar

Scanning electron microscopy (SEM) has been used analyses the surface morphology of SCL biochar and the resulting micrographs are shown in Fig. 6.11a. This picture shows the numerous biochar pores and cracks on the surface; this indicates the decrease in volatile matter of biomass during pyrolysis. The bio-char EDX study was conducted to determine the surface point Composition of elementals. Fig. 6.11(b) shows the bio-char EDX spectra that indicate the presence of N, C, Mn, Ca, Si, Al and Mg in the bio-char.

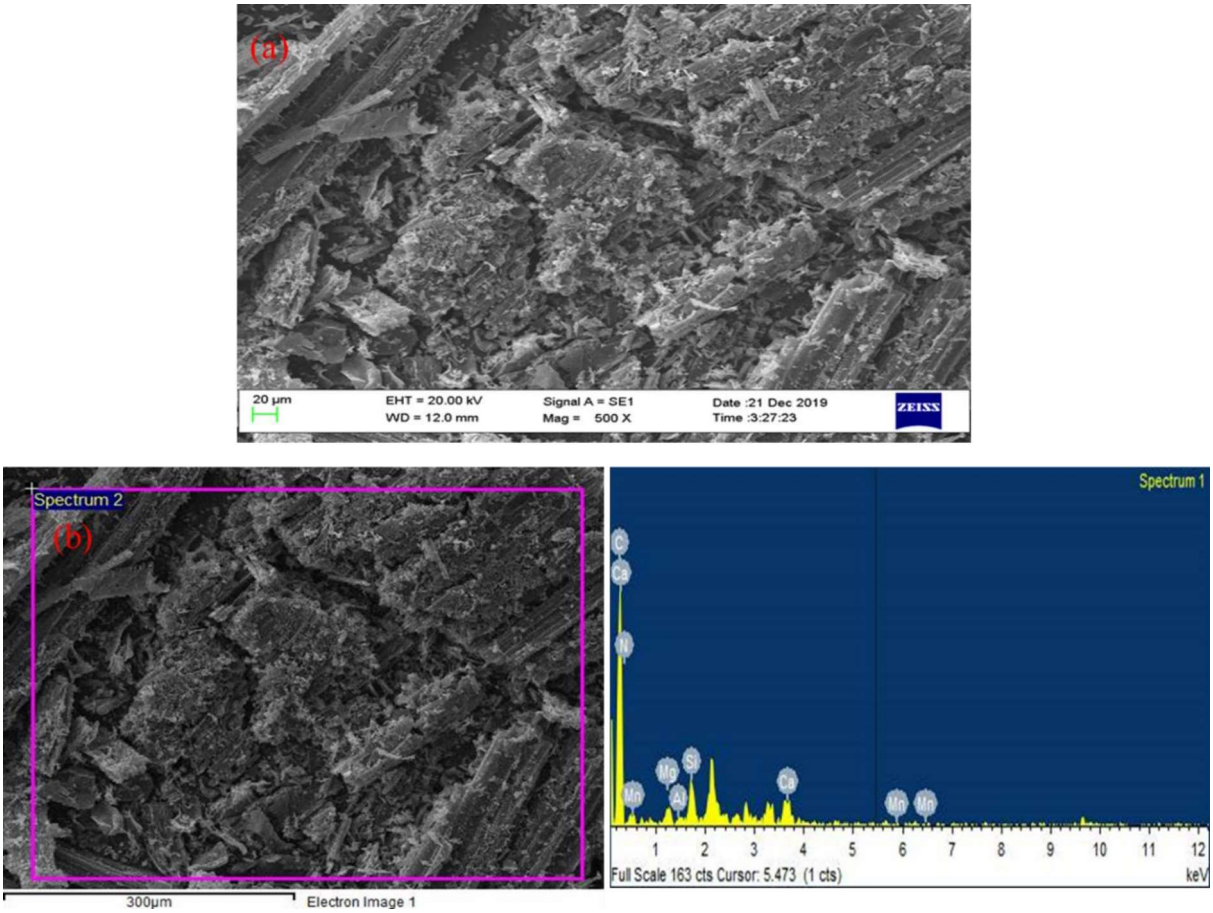

Fig. 6.11 (a) FESEM image of bio-char (b) EDX spectra of bio-char

6.7.10.3 ICP-AES analysis of biochar

ICP analysis of biochar was carried out in order to investigate the quantity of mineral content in the biochar. Moreover, analysis by ICP-AES was performed in order to verify the metal content in the biochar and thus determine the viability of the biochar as a source of nutrients for soil (N, P, K, Fe, etc.).The constituents of biochar are reported in Table 6.7.

6.7.10.4 FTIR spectra of SCL biochar

To analysis the functional group present in biochar after pyrolysis of SCL, FTIR analysis has been performed. FTIR spectra of biochar in the wavenumber range of 500 to 4000cm^{-1} are presented in Fig. 6.9. The wider band is assigned to the O-H group in the wavenumber range of 3600-3200cm^{-1}, which attributes the presence of water, alcohol and phenol (Yang et al., 2007). The aliphatic C-H stretching was due to a low intensity peak at 2900cm^{-1} (Angın, 2013). The peaks represent the presence of carboxyl groups in the band gap of 2300– 2000cm^{-1}(Moralı and Sensöz, 2015). The lower intensity peak observed around 1590cm^{-1} reveals the vibration of C=C stretching and the presence of alkenes and aromatics in the SCL biochar. The lower peak at approximately 1200cm^{-1} corresponds to the C-H bending vibration, suggesting the presence of alkanes (Balagurumurthy et al., 2015). The stretching vibrations of aromatic C-H are due to very small peak in the range of 1000-700cm^{-1}; these bands reflect the presence of aromatic hydrogen in the biochar (Yakkala et al., 2013).

6.7.10.5 Thermal Stability of biochar

Thermal behaviour of biochar produced during pyrolysis of SCL was studied using thermogravimetric analysis (TGA) and differential thermogravimetric analysis (DTG) and these profiles are showing in Fig. 6.12. It was found that the weight loss of approximate 10% of biochar up to 150^{o} at a rate of 0.7%/min. this weight loss only due to the adsorb moisture from the environment. After 150^{o}C, there was hardly weight loss observed up to 450^{o}C on the other hand in the raw SCL maximum weight dropped up to 450^{o}C. These activities indicate the thermal stability of SCL of biochar. High rate of degradation for raw

SCL started approximately at 250 °C whereas for SCL char took place after 450°C. The highest degradation rate occurred at approximately 575°C for SCL biochar. The previous statement that the SCL biochar could withstand a higher temperature further confirms these findings. The maximum weight loss in the temperature range of 450 to 600ºC is mainly due to residual component of biochar (hemicellulose, cellulose and lignin) Similar finding were also observed by Mazlan et al., (2015) for Meranti wood sawdust (MWS) biochar and Salgado et al., (2017) for Babassu endocarp biochar.

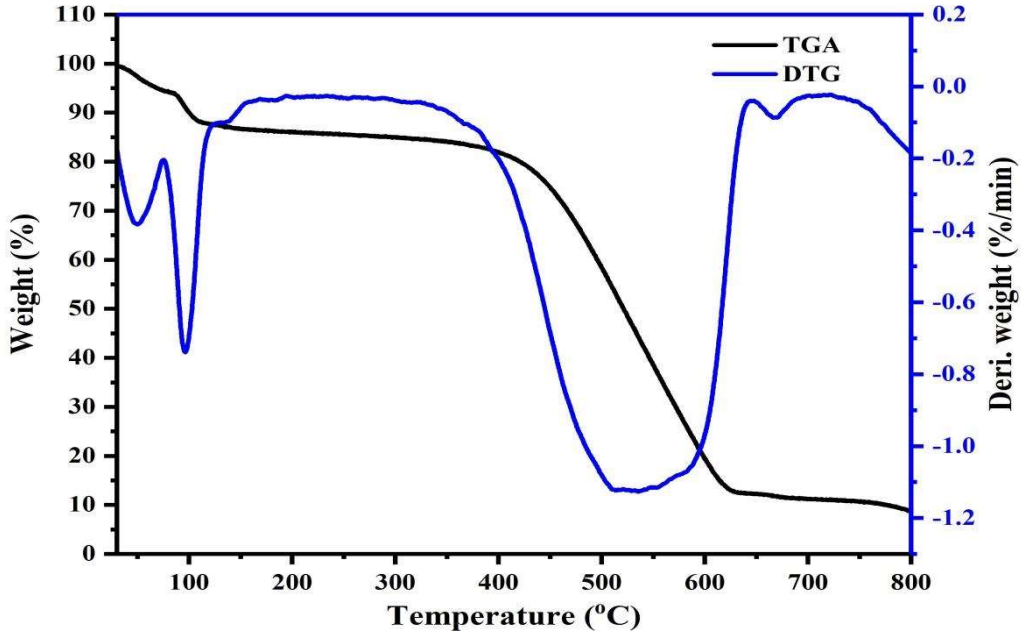

Fig. 6.12 TGA and DTG curves of bio-char at a heating rate of 15ºC/min

6.7.11 GC analysis

GC-TCD and GC-FID have been used to study the variations in pyrolytic non- condensable gas composition from SCL pyrolysis at different temperatures are shown in Fig. 6.13(a). Fig 6.13(a) indicates that the generated gas primarily contains hydrogen (H_2), methane (CH_4), carbon monoxide (CO) and carbon dioxide (CO_2). H_2 has been detected using GC-

TCD where CO, CO_2 and CH_4 detected using GC-FID. Initially at lower temperature (up to 415^oC) the composition of CO and CO_2 was higher as compared to other constituents of gas. This is attributed to the degradation of hemicellulose and cellulose and these components of biomass more or less degraded up to 500^oC (Dhyani and Bhaskar, 2018). Another possible functional group of CO_2 release are C=O and COOH which is present in raw SCL (Jahirul et al., 2012). Release of CO_2 at higher temperature is also continuing and this may be due to the decomposition of lignin. It can be seen from Figure that the concentration of CO in the gas mixture decreases with increase in temperature in the order of 20.62% at 300^oC to 3.74% at 600^oC. Generation of CO is possibly due to the thermal decomposition of the carbonyl (C-O-C) and carboxyl (C=O) groups below 500^oC and at higher temperature it is due to the lignin degradation. Therefore, it can be conclude that the presence of oxygen content in raw SCL sample during CHNS analysis is due to the present of this functional group while the pyrolysis experiment is carried out in presence of inert atmosphere. Therefore cellulose and hemicellulose are also mainly component for releasing CO and CO_2. Fig 6.13(a) shows that the concentration of CH_4 increases (from 4.10% at 300oC) with temperature up to 500^oC (38.55%) and then decrease to 0.28% at 600^oC. The release of CH_4 from pyrolysis of SCL is mainly due to the decomposition of methoxy (O-CH_3) group (Yang et al., 2007). The concentration of H_2 continuously increases from 5.93% at 300^oC to 79.07% at 600^oC. The hydrogen release was primarily due to the cracking and decomposition of aromatic rings and lignin methoxy groups (Gupta et al., 2019).

The Variation of HHV of non-condensable pyrolytic gas with temperature is depicted in Fig 6.13(b). It is crucial to know the HHV of pyrolytic gas as it explains its ability to be

used as fuel. High combustion properties are given by the presence of methane and hydrogen in the gas composition and can be used for energy production. The HHV of pyrolytic gases was estimated using the formula provided by Guangul et al. (2014) at different temperatures. It can be seen from Fig. that the HHV of the gas increases from 5007.20kJ/Nm^3 at 300^{o}C to 20876.85kJ/Nm^3 at 550^{o}C then decrease to 10721.29kJ/Nm^3 at 600^{o}C. The reduction in HHV of gas is due to the lesser production of methane at higher temperature as discussed in earlier section. In order to provide process heat for various operations, the pyrolytic gas may be combusted. It can also be processed to increase the yield of bio-oil and its properties (Mante et al., 2012; Dhyani and Bhaskar, 2018).

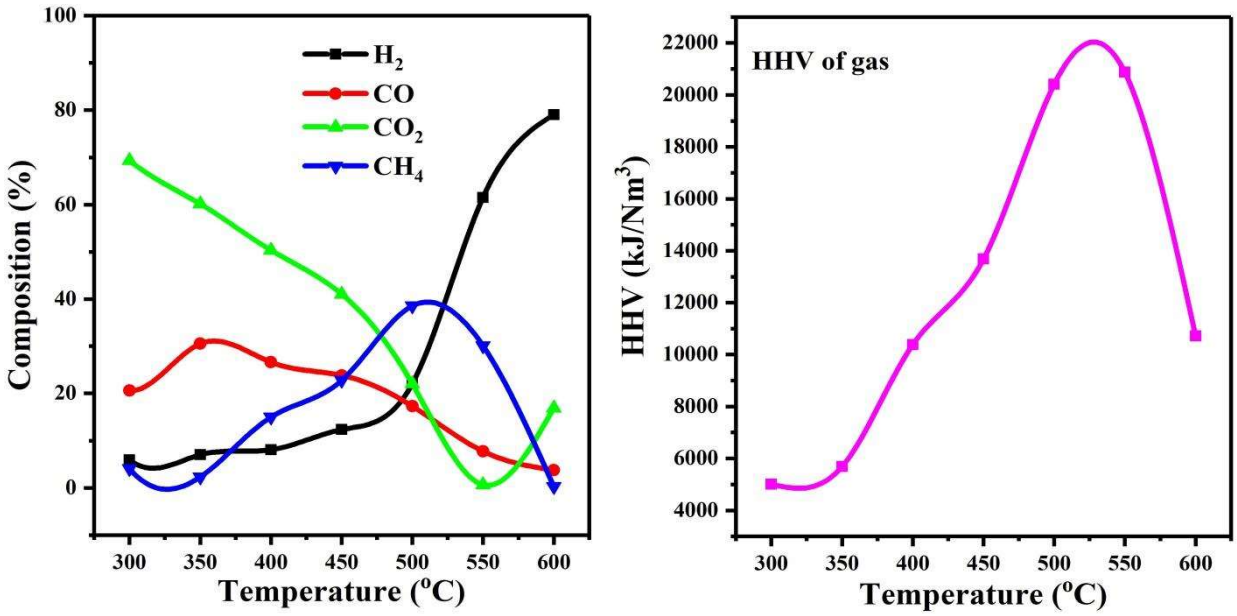

Fig. 6.13 Non-condensable gas fraction (a) composition (b) Higher heating value (HHV) at different pyrolysis temperature

6.8 Conclusion

Thermal degradation kinetics of sugar cane leaves has been investigated using TGA/DTA. The model-free methods are better than the regression analysis method in representing the

thermal degradation kinetics. The Vyazovkin AIC model-free method has been found to be better compared to other models. The activation energy has been found to vary with conversion indicating the complex multi-step nature of the thermal degradation kinetics. For conversion values below 0.2 the thermal degradation process is controlled by the nucleation and growth mechanisms and the reaction follows between 1.04 and 1.41 order kinetics. The higher yield of liquid product was found to be 44.78wt% at temperature of 550^{o}C, heating rate 25^{o}C/min. bed height of 16cm and particle size in the range of 0.300-0.180mm. Product distribution demonstrated that the liquid yield was increases up to 550^{o}C and decreases after that on the other hand the gaseous products yield raises and biochar yield reduces continuously with increase in temperature. It was noted that the liquid yield increases with heating rate and maximum at 25^{o}C/min thereafter decreased while biochar decreases continuously. The yield of liquid product was also increases with increases in bed height while decreases with increase in the range of particle size. Characterization of liquid product and their different properties indicated that it can be useful for fuel and various value added chemicals after necessary refining and up gradation. As a solid fuel and a precedent for activated carbon, biochar may also be used. It also assists in increasing crop production through the neutralization of soil acidity. The present study concludes that SCL is a strong potential source of renewable energy for pyrolysis; if all the pyrolysis products are used competently.